STATISTICS, OPTIMIZATION AND INFORMATION COMPUTING
Stat., Optim. Inf. Comput., Vol. **16**, August 2026, pp 1716–1726.
Published online in International Academic Press (www.IAPress.org)

Numerical Study of Compressible Newtonian Fluid Flow with Low Viscosity in a Lid-Driven Cavity

Hassan Khaleel Ismail [1], Hayder Abbas Janabi [2], Anas Al-Haboobi [1,*]

[1] *Department of Mathematics, Faculty of Computer Sciences & Mathematics, University of Kufa, Kufa, Iraq*
[2] *Department of Basic Sciences, Faculty of of Dentistry, University of Kufa, Kufa, Iraq*

Abstract This paper focuses on numerical analysis of Newtonian compressible fluid flow in a square cavity driven by a lid, where the motion of the fluid is generated by moving the upper wall with prescribed velocity. The numerical solution of the governing equations is performed within a Taylor–Galerkin/Pressure–Correction finite element framework (TGPC). The pattern of the flow is governed by Navier–Stokes equations, consisting of the continuity equation describing mass conservation and unsteady momentum equations written in Cartesian coordinates. The objective of this work is to investigate the role of low dynamic viscosity (μ) on some significant flow properties. The influence of the viscosity change on the velocity field, shear stress, pressure and density distributions is investigated in details. Numerical solutions show that, when (μ) is increased, the trajectory of velocity becomes smaller in magnitude, whereas the other hydrodynamic profiles become larger. In general, the expected tendencies are in qualitative agreement with basic physical principles of viscous compressible flows.

Keywords Speed of sound, Compressible flow, Taylor–Galerkin/ Pressure–Correction, Lid-driven cavity, Finite element method.

AMS 2010 subject classifications 76M10, 76Nxx, 76A05.

DOI: 10.19139/soic-2310-5070-3507

1. Introduction

A compressible fluid is distinguished by changes in density produced under the influence of pressure or temperature. Such fluids are predominantly gases, such as air, in contrast to incompressible fluids, most liquids, whose density remains nearly constant under typical flow conditions. The study of compressible flows is crucial in high-speed engineering devices such as jet propulsion engines, aerospace vehicles and gas turbines in which the compressibility effects cannot be ignored [1, 2].
The fundamental differences between compressible and incompressible fluids lead to a considerable mathematical and numerical complexity of the governing equations. Accordingly, much research has been spent on implementing and evaluating robust numerical schemes for the computation of compressible flows. In fact, the study of fluid flow in the context of canonical geometries is vital for elucidating flow physics for practical applications in industrial processes like rocket nozzles, jet engines or combustion chambers [3].
The compressible flows of newtonian fluids in a lid-driven cavity has been extensively investigated in fluid mechanics. and are numerically simulated by solving the differential equations for those flows. These flows are governed by the conservation of time-dependent mass and momentum conservation equations, have been expressed generally in Cartesian coordinates for isothermal conditions [4, 5, 6]. Although it may appear to be a simple geometry, the lid-driven cavity is a classical one and has great practical and theoretical value in numerous

*Correspondence to: Anas Al-Haboobi (Email: anasm.ali@uokufa.edu.iq).

ISSN 2310-5070 (online) ISSN 2311-004X (print)

engineering applications. In this work, the case of square lid-driven cavity is taken as a representative test case. This setup is a model of several engineering problems including flows over recessed surfaces, cuts, and multiple slots along aircraft fuselages or heat exchangers. There are several types of lid-driven cavity flows based on the imposed boundary conditions, such as single-wall driven, parallel-wall driven, and anti-parallel-wall driven flows, as discussed in [7]. This study is attention to the single upper wall-driven case where the fluid motion is driven by the motion of the lid at a prescribed constant velocity.

The lid-driven cavity problem has been extensively investigated as a benchmark numerical problem and as a test platform for analyzing specific physical effects in both compressible and incompressible flow regimes [8]. Numerous numerical studies addressing steady incompressible cavity flows have been reported in the literature, employing a variety of numerical techniques and serving as reference solutions for method validation and comparison. Khalaf et. al., [9] study incompressible flow in square lid-driven cavity with hemispherical obstacle. Finite volume method was used to solve the incompressible flow in lid-driven problem by Patel et. al., [10]. Lid-driven problem with with nanofluids was investigated by Borbora et. al., [11]. Khalid et. al., [12] study lid-driven problem with incompressible flow under thermal conditions. Our work distinguishes previously performed studies, is our study focus on compressible fluid in lid-driven cavity, a relatively new and insufficiently explored field, in addition to the use of the Taylor-Gallerkin/Pressure Correction (TGPC) method and its high accuracy and efficiency in solving fluid-associated fluids.

The main contribution of this work lies in the application of the Taylor–Galerkin/pressure-correction (TGPC) method to obtain numerical solutions of compressible Newtonian fluid flow in a lid-driven cavity under isothermal conditions. This study is the first of its kind to investigate a compressible fluid within a lid-driven cavity , as previous studies have focused exclusively on incompressible fluids. This allowed us to study the properties of this type of fluid and understand it better within this type of geometric shape, while comparing it to a fluid in its incompressible state. The proposed numerical framework is specifically designed for fluid dynamics applications and provides a reliable tool for evaluating the accuracy and effectiveness of the TGPC method in monitoring compression effects in Newtonian flows.

From a numerical perspective, a semi-implicit Taylor–Galerkin/pressure-correction finite element method (TGPC) is employed for temporal discretization. This formulation was originally introduced by Townsend and Webster [13] to treat incompressible Newtonian and non-Newtonian flows. Within this approach, the velocity and pressure fields are decomposed following a primitive-variable formulation, an idea inspired by the investigations of Chorin [14]. Owing to its robustness and second-order temporal accuracy, this method has attracted considerable interest for the treatment of a wide range of flow problems see [15, 16, 17, 18, 19].

The primary motivation of the present study is to extend the TGPC methodology to compressible flow problems formulated in Cartesian coordinates. To this end, the classical square lid-driven cavity benchmark is adopted as a test configuration. The main numerical findings focus on examining the influence of the squared speed of sound (c^2) on different main components. These investigations provide new insights into the interplay between compressibility and viscosity in confined Newtonian flows.

2. Mathematical modeling

The non-dimensionalized governing equations for mass and momentum conservation describing compressible Newtonian flow under isothermal conditions are given by [18]:

$$\frac{\partial \rho}{\partial t} + Re\nabla \cdot (\rho \upsilon) = 0, \tag{1}$$

$$\rho Re(\frac{\partial \upsilon}{\partial t} + (\upsilon \cdot \nabla \upsilon)) = \nabla \cdot (\mu(\nabla \upsilon + \nabla \upsilon^T)) - \frac{2}{3}\nabla(\mu \nabla \cdot \upsilon) - \nabla p. \tag{2}$$

Where (ρ, p, υ and μ) denoted the fluid density, pressure, velocity vector and dynamic viscosity, respectively. Re is a dimensionless parameter, known as the Reynolds number, defined as [19]:

$$Re = \frac{\rho^0 \upsilon^0 L}{\mu}. \tag{3}$$

Since the fluid under consideration is compressible, its density is not constant but varies with pressure. Consequently, it is necessary to establish a constitutive relationship between pressure and density in order to evaluate the density field required for closing the governing equations of mass and momentum conservation. To this end, the modified Tait equation of state [20] is adopted and expressed in the following form:

$$\frac{p+\beta}{p_0+\beta} = (\frac{\rho}{\rho_0})^{\kappa}, \tag{4}$$

where κ and β are model parameters and ρ, ρ_0 denote the instantaneous and reference densities, respectively. Differentiating Eq.4 with respect to ρ, yields:

$$\frac{\partial p}{\partial \rho} = \kappa \rho^{\kappa-1} \frac{p_0+\beta}{\rho_0^{\kappa}} = \frac{\kappa(p+\beta)}{\rho} = c^2_{(x,t)}, \tag{5}$$

$$\frac{\partial \rho}{\partial t} = \frac{\partial \rho}{\partial p}\frac{\partial p}{\partial t} = \frac{1}{c^2_{(x,t)}}\frac{\partial p}{\partial t}. \tag{6}$$

3. Problem Specifiction and Boundary Conditions

3.1. Problem Specifiction

To validate the proposed numerical approach, an important benchmark problem within the framework of compressible Newtonian flows is considered. As illustrated in Figure 1, a lid-driven cavity configuration is examined, in which the fluid motion is induced by the uniform translation of the upper wall (lid) at a prescribed velocity. For the spatial discretization, a (25×25) structured triangular finite element mesh is employed, consisting of 1308 elements, 701 nodal points, and a total of 2103 degrees of freedom. This benchmark configuration provides a reliable basis for assessing the accuracy and robustness of the proposed formulation.

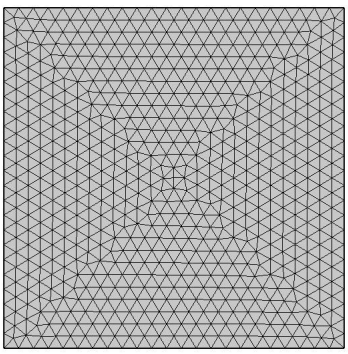

Figure 1. Problem geometry and mesh.

3.2. Boundary Conditions

The setting of the problem under consideration put as follows:

1. At the upper boundary, the tangential velocity with a variable profile of type $U = 16x^2(1-x^2)$ is applied to drive the fluid flow in the cavity.
2. No-slip BCs is applied on the remaining three walls.

4. Numerical technique

In this study, a time semi-implicit Taylor–Galerkin/pressure-correction (TGPC) numerical scheme is employed. The method is formulated within a fractional-stage framework, in which the temporal discretization is initially performed using Taylor series expansions. A two-step Lax–Wendroff procedure is incorporated to achieve second-order accuracy in time. Subsequently, a modified operator-splitting strategy, known as the pressure-correction technique, is applied to decouple the velocity and pressure fields.
The pressure-correction approach was originally introduced by Van Kan [21], who demonstrated that the method attains second-order temporal accuracy and enhanced numerical stability through linear energy analysis. Historically, Taylor–Galerkin schemes were first proposed in explicit form by Hawken et al. for incompressible flow simulations. Later, Townsend and Webster [13] formalized the combined Taylor–Galerkin/pressure-correction framework, which has since become known as the TGPC method.
The equation for momentum conservation becomes

$$\text{step 1:}\frac{2\rho Re}{\Delta t}[v^{n+\frac{1}{2}}-v^n] = \nabla(\mu(\nabla v^n + (\nabla v^n)^T)) - \frac{2}{3}\nabla(\mu(\nabla v^n)) - \rho Re(v^n\cdot\nabla v^n) - \nabla p^n, \tag{7}$$

$$\text{step 2:}\frac{\rho Re}{\Delta t}[v^{n+1}-v^n] = \nabla(\mu(\nabla v^{n+\frac{1}{2}} + (\nabla v^{n+\frac{1}{2}})^T)) - \frac{2}{3}\nabla(\mu(\nabla v^{n+\frac{1}{2}})) - \rho Re(v^{n+\frac{1}{2}}\cdot\nabla v^{n+\frac{1}{2}}) - \nabla p^{n+\frac{1}{2}}. \tag{8}$$

The pressure $p^{n+\frac{1}{2}}$ in Eq.8 is approximated by

$$p^{n+\frac{1}{2}} = \lambda p^{n+1} + (1-\lambda)p^n. \tag{9}$$

In this case, the pressure $p^{n+\frac{1}{2}}$ has an error equal to $O(\Delta t^2)$ for $\lambda = \frac{1}{2}$ while possessing an error equivalent to $O(\Delta t)$ for other values of λ, $p^{n+\frac{1}{2}}$. Eq.8 can therefore be written as

$$\frac{\rho Re}{\Delta t}[v^{n+1}-v^n] = \nabla(\mu(\nabla v^{n+\frac{1}{2}} + (\nabla v^{n+\frac{1}{2}})^T)) - \frac{2}{3}\nabla(\mu(\nabla v^{n+\frac{1}{2}})) - \rho Re(v^{n+\frac{1}{2}}\cdot\nabla v^{n+\frac{1}{2}}) - \lambda p^{n+1} + (1-\lambda)p^n. \tag{10}$$

We suggest a velocity v^* to solve Eq.10 in combination with the compressibility Eq.1, so that

$$\frac{\rho Re}{\Delta t}[v^*-v^n] = \nabla(\mu(\nabla v^{n+\frac{1}{2}} + (\nabla v^{n+\frac{1}{2}})^T)) - \frac{2}{3}\nabla(\mu(\nabla v^{n+\frac{1}{2}})) - \rho Re(v^{n+\frac{1}{2}}\cdot\nabla v^{n+\frac{1}{2}}) - \nabla p^n. \tag{11}$$

Now, by subtracting Eq.11 from Eq. 10, we have

$$\frac{\rho Re}{\Delta t}[v^{n+1}-v^*] = -\lambda\nabla(p^{n+1}-p^n). \tag{12}$$

Using Eq. 1 and the divergence of the two sides of Eq. 12, we get

$$\frac{\Delta\rho^{n+1}}{\Delta t} + \nabla\cdot(\rho Re\upsilon^*) = \lambda\Delta t\nabla^2(p^{n+1}-p^n). \tag{13}$$

Furthermore, by applying the chain rule to Eq. 5 and carrying out different operations, we may link the rise in density to the rise in pressure by

$$\frac{\Delta\rho^{n+1}}{\Delta t} = \frac{1}{c^2_{(x,t)}}\frac{\Delta p^{n+1}}{\Delta t}. \tag{14}$$

By substituting Eq. 14 into Eq. 13, we obtain

$$\frac{1}{c^2_{(x,t)}}\frac{\Delta p^{n+1}}{\Delta t}\nabla\cdot(\rho Re\upsilon^*) = \lambda\Delta t\nabla^2(p^{n+1}-p^n). \tag{15}$$

Thus, from the equations 7, 11, 12, 14 and 15, we can solve the system of compressible equations (mass and momentum) in the following order:

$$\text{stage 1:}\quad \frac{2\rho Re}{\Delta t}[\upsilon^{n+\frac{1}{2}}-\upsilon^n] = \nabla(\mu(\nabla\upsilon^n+(\nabla\upsilon^n)^T)) - \frac{2}{3}\nabla(\mu(\nabla\upsilon^n)) - \rho Re(\upsilon^n\cdot\nabla\upsilon^n) - \nabla p^n, \tag{16}$$

$$\text{stage 2:}\frac{\rho Re}{\Delta t}[\upsilon^*-\upsilon^n] = \nabla(\mu(\nabla\upsilon^{n+\frac{1}{2}}+(\nabla\upsilon^{n+\frac{1}{2}})^T)) - \frac{2}{3}\nabla(\mu(\nabla\upsilon^{n+\frac{1}{2}})) - \rho Re(\upsilon^{n+\frac{1}{2}}\cdot\nabla\upsilon^{n+\frac{1}{2}}) - \nabla p^n, \tag{17}$$

$$\text{stage 3:}\quad \frac{1}{c^2_{(x,t)}}\frac{\Delta p^{n+1}}{\Delta t}\nabla\cdot(\rho Re\upsilon^*) = \lambda\Delta t\nabla^2(p^{n+1}-p^n), \tag{18}$$

$$\text{stage 4:}\quad \frac{\Delta\rho^{n+1}}{\Delta t} = \frac{1}{c^2_{(x,t)}}\frac{\Delta p^{n+1}}{\Delta t}, \tag{19}$$

$$\text{stage 5:}\quad \frac{\rho Re}{\Delta t}[\upsilon^{n+1}-\upsilon^*] = -\lambda\nabla(p^{n+1}-p^n). \tag{20}$$

The finite element weak formulation, incorporating suitable approximations for the velocity, pressure, and density fields at all stages of the algorithm, can be expressed as follows:

$$\text{Stage 1:}\frac{2\rho Re}{\Delta t}\int_\Omega\Big[\sum_{j=1}^n\upsilon_j^{n+1}\Phi_j(x)-\sum_{j=1}^n\upsilon_j^n\Phi_j(x)\Big].\Phi_i d\Omega = \int_\Omega\Big[\sum_{j=1}^n p_j^n\Psi_j\Big]\nabla\cdot\Phi_i d\Omega - \mu\int_\Omega\Big[\sum_{j=1}^n\nabla\upsilon_j^n\nabla\Phi_j + \sum_{j=1}^n(\nabla\upsilon^n)^T(\nabla\Phi_j)^T\Big]\nabla\Phi_i d\Omega + \frac{2}{3}\mu\int_\Omega\Big[\nabla\sum_{j=1}^n\upsilon^n\Phi_j\Big]\nabla\Phi_i d\Omega - \rho Re\int_\Omega\Big[\sum_{j=1}^n\upsilon_j^n\Phi_j\cdot\nabla\sum_{j=1}^n\upsilon_j^n\Phi_j\Big]\Phi_i d\Omega,$$

$$\text{Stage2:}\frac{\rho Re}{\Delta t}\int_\Omega\Big[\sum_{j=1}^n\upsilon_j^*\Phi_j(x)-\sum_{j=1}^n\upsilon_j^n\Phi_j(x)\Big].\Phi_i d\Omega = \int_\Omega\Big[\sum_{j=1}^n p_j^n\Psi_j\Big]\nabla\cdot\Phi_i d\Omega - \mu\int_\Omega\Big[\sum_{j=1}^n\nabla\upsilon_j^{n+\frac{1}{2}}\nabla\Phi_j + \sum_{j=1}^n(\nabla\upsilon^{n+\frac{1}{2}})^T(\nabla\Phi_j)^T\Big]\nabla\Phi_i d\Omega + \frac{2}{3}\mu\int_\Omega\Big[\nabla\sum_{j=1}^n\upsilon^{n+\frac{1}{2}}\Phi_j\Big]\nabla\Phi_i d\Omega - \rho Re\int_\Omega\Big[\sum_{j=1}^n\upsilon_j^{n+\frac{1}{2}}\Phi_j\cdot\nabla\sum_{j=1}^n\upsilon_j^{n+\frac{1}{2}}\Phi_j\Big]\Phi_i d\Omega,$$

$$\text{Stage3: } \int_\Omega \Big[\sum_{j=1} \rho^n \Psi_j Re \nabla \sum_{j=1}^{n} \upsilon_j^* \Phi_j\Big] \Psi_i d\Omega = -\lambda \Delta t \int_\Omega \Big[\nabla \sum_{j=1}^{n} (p^{n+1} - p^n)\Psi_j\Big] \Psi_i d\Omega - \frac{1}{c^2_{(x,t)}} \frac{1}{\Delta t} \int_\Omega \Big[\nabla \sum_{j=1}^{n} p^{n+1} \Psi_j\Big] \Psi_i,$$

$$\text{Stage 4: } \frac{1}{\Delta t} \int_\Omega \Big[\sum_{j=1}^{n} \Delta p^{n+1} \Psi_j\Big] \Psi_i d\Omega = \frac{1}{c^2_{(x,t)}} \frac{1}{\Delta t} \int_\Omega \Big[\sum_{j=1}^{n} \Delta p^{n+1} \Psi_j\Big] \Psi_i d\Omega,$$

$$\text{Stage 5: } \frac{\rho^n Re}{\Delta t} \int_\Omega \Big[\sum_{j=1}^{n} \upsilon^{n+1} \Phi_j - \sum_{j=1}^{n} \upsilon^* \Phi_j\Big] \cdot \Phi_i d\Omega = \lambda \int_\Omega \Big(\sum_{j=1}^{n} p^{n+1} \Psi_j - \sum_{j=1}^{n} p^n \Psi_j\Big) \nabla \Phi_i d\Omega.$$

5. Computational Results

In the present study, a lid-driven cavity configuration is employed as a benchmark problem to validate and calibrate the proposed numerical algorithm. The numerical study focuses on exploring compressible Newtonian fluids, primarily investigating the effect of low viscosity (μ) on velocity, shear stress, and density with multiple variations with respect to the speed of sound. The key findings examine how viscosity influences the horizontal and vertical velocity components along the cavity centerlines, in addition to impacting the shear stress along its bottom wall. Systematic importance of pressure and density variations are also investigated. To this end, a time fractional-staged Taylor–Galerkin/Pressure–Correction (TGPC) framework is used. All numerical simulations are performed in the Cartesian coordinates.

5.1. Speed of Sound variations

In this subsection the effect of sound speed on density, expressed above in terms of pressure dependence in Eq. 6 is explored. Table 1 summarizes the effect of varying $c^2 = \{100, 500, 1000\}$ on the density field. Clearly it is an inverse relationship as the speed of sound increases, density variations decrease. For all the subsequent simulations, the value $c^2 = 1000$ is used, based on these observations, to obtain the regime that is closest to incompressible flow behavior. Based on these observations, the value $c^2 = 1000$ is used in all the subsequent simulations to obtain the regime that is closest to the incompressible flow behavior [22].

Table 1. Effect of speed of sound at $\mu = 0.05$ on density.

c^2	ρ
100	0.0148
500	2.96×10^{-3}
1000	1.48×10^{-3}

5.2. Viscosity variations

Viscosity (μ) is a key rheological parameter, which influences substantially in the flow of the fluid. Viscosity is a key parameter governing fluid flow and energy dissipation and it directly affects the flow of fluids and the dissipation of energy and momentum. Also, accurate characterization of the viscous effects is important for engineering systems and industrial processes where the fluid flow plays a significant role in their design, control, and optimization. For this reason, the study of the viscosity effect is carried out by varying the viscosity parameter μ = [0.01, 0.05, 0.1] and observing the effect of these variations on the main flow quantities.

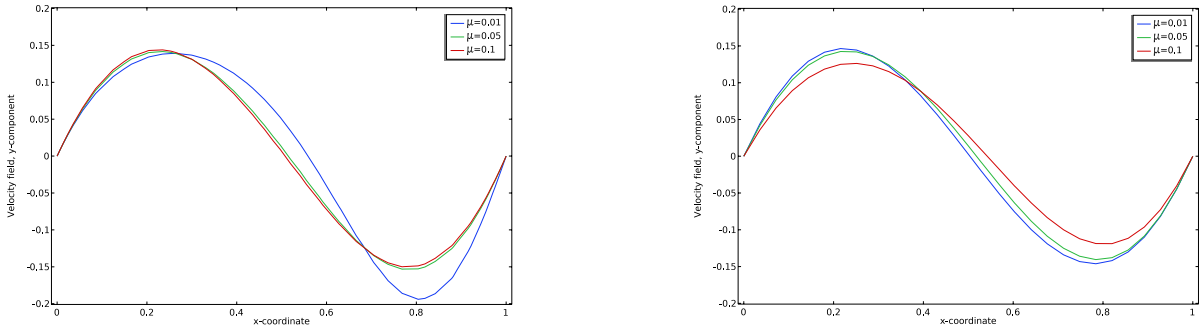

Incompressible case Compressible case

Figure 2. Effect of different values of μ on velocity profile along the vertical centreline of the cavity for both incompressible and compressible cases.

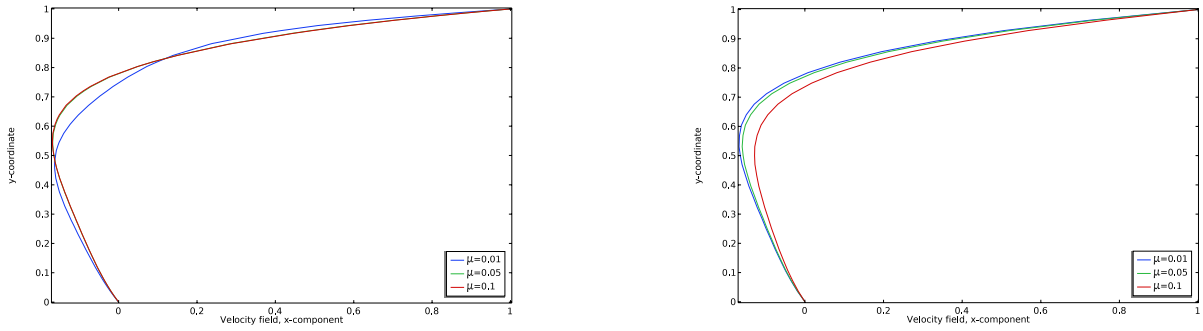

Incompressible case Compressible case

Figure 3. Effect of different values of μ, on velocity profile along the horizontal centreline of the cavity for both incompressible and compressible cases.

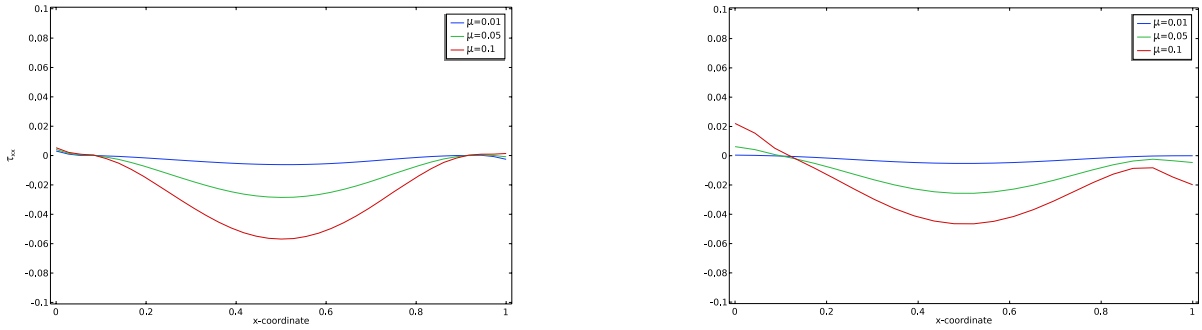

Incompressible case Compressible case

Figure 4. Effect of different values of μ, on τ_{xy} profile for both incompressible and compressible cases.

A comparative analysis is done between compressible and incompressible flow in order to explain the role of the viscous forces in a different state of compressibility. The impact of dynamic viscosity μ on velocity distribution along the horizontal and vertical centerlines of the cavity in both incompressible and compressible flow regimes is shown in figures 2 and 3 respectively. The results show that the higher the value of μ, the smaller the velocity magnitudes are because of the increased internal resistance to flow [23]. Additionally, the level of velocity field

attenuation is higher for the incompressible flow case compared to the compressible flow case, indicating the damping effect of compressibility effects on momentum diffusion.

As is evident in Figure 4 the shear stress for τ_{xy} is always increasing as the viscosity μ increases, and this increase is particularly marked in the incompressible flow region. This has been attributed to better viscous shear and compressibility effects on momentum diffusion, , as discussed by Zaidi [24].

As you can see in the streamline pattern (Figure. 5) the greater the viscosity (μ) the more we have damping of velocity near the center of the vortex core and the weaker we have the strength of rotating flow. This leads to the production of smaller and weaker vortical structures (especially incompressible flow). The higher the value of the μ the greater the viscous forces, or the more energy is dissipated and the more resistance to the particle motion, which results in a slower flow speed and less energy in the vortices.

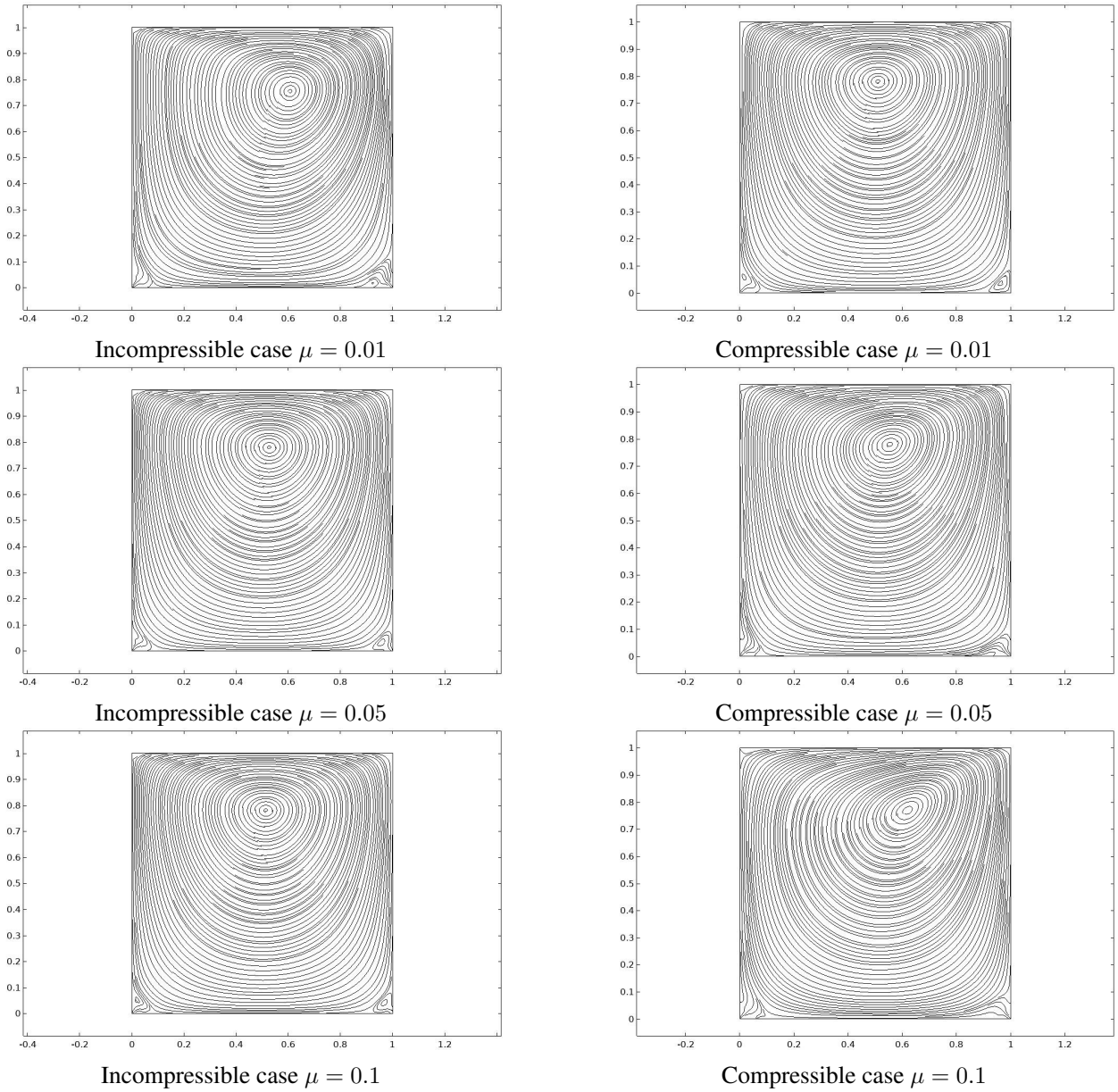

Figure 5. Streamline patterns for velocity flow; μ-variation at both incompressible and compressible cases.

The effect of μ on the pressure field is shown in Figure 6 for both compressible and incompressible flow. They show that the pressure levels increase systematically with an increase in μ, being more significant for the incompressible regime. In compressible flows, this pressure–viscosity coupling is relatively weak, with the ability to accept higher levels of flow resistance being provided by the compressibility of the fluid, see [23].

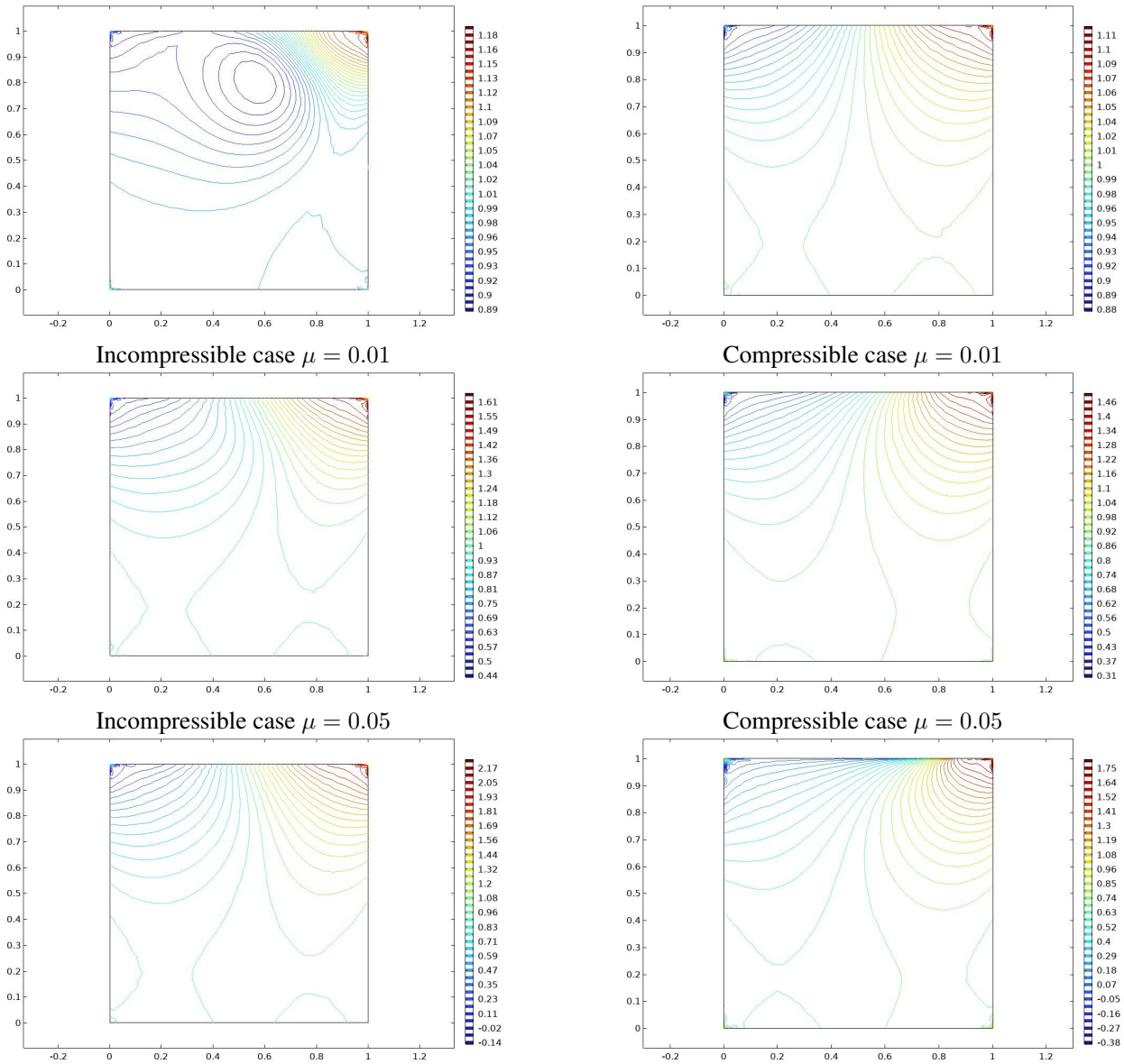

Figure 6. Pressure contours for various μ for both incompressible and compressible cases.

In terms of the density field, Figure 7 shows that as the viscosity μ increases, so do the densities, as the resistance to deformation increases.

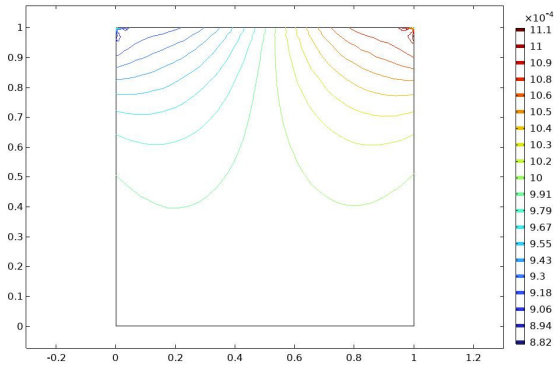

Compressible case $\mu = 0.01$

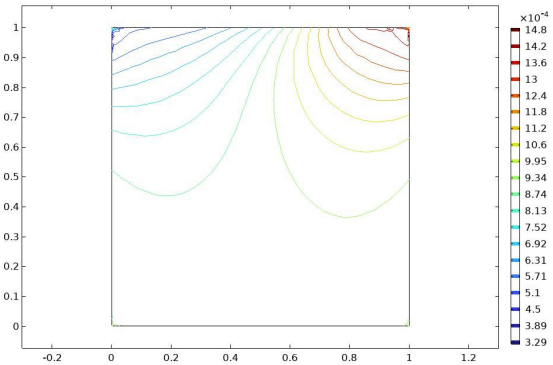

Compressible case $\mu = 0.05$

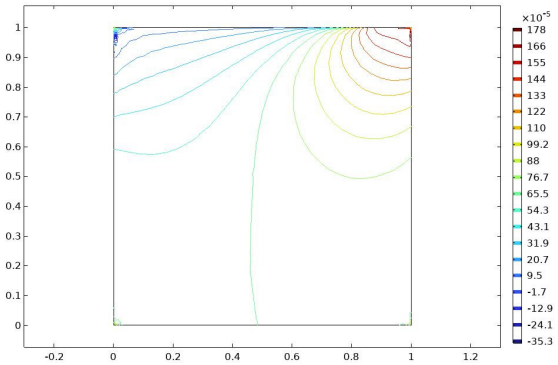

Compressible case $\mu = 0.1$

Figure 7. Density contours for various μ.

6. Conclusions

In this study, numerical simulations of low-viscosity compressible Newtonian fluid flow are conducted within a two-dimensional square cavity driven by a moving top lid at a prescribed velocity. The governing equations are solved using the Taylor–Galerkin/pressure-correction finite element method (TGPC), which is well suited for compressible flow simulations. To evaluate the fluid density, a pressure–density relationship based on the modified Tait equation of state is introduced. This relation is analytically derived and consistently incorporated into the fractional stages of the TGPC algorithm. The numerical computations are performed on a structured finite element mesh consisting of a 25×25 grid. A parametric investigation is carried out to examine the influence of the squared speed of sound (c^2) on density variations. The findings show that when c^2 is increased, density fluctuations decrease, suggesting the flow behavior gradually changes towards the incompressible limit. Moreover, the impact of low dynamic viscosity on the main flow quantities is investigated between compressible and incompressible fluids. The results indicate that the incompressible scenario brings about more relevant and salient viscosity-controlled effects. All the numerical results are consistent with known physical behaviour and in excellent agreement with those published earlier in the literature, affirming the reliability and validity of the developed numerical scheme.

REFERENCES

1. G. A. Al-Juaifri and A. J. Harfash, *Existence and uniqueness of solution for the nonlinear Brusselator system with Robin boundary conditions*, Georgian Mathematical Journal, vol. 31, no. 3, pp. 355–368, 2024. doi: 10.1515/gmj-2023-2091.
2. G. A. Al-Juaifri and A. J. Harfash, *Numerical analysis of the Brusselator model with Robin boundary conditions*, SeMA Journal, vol. 82, no. 3, pp. 351–397, 2025. doi: 10.1007/s40324-024-00361-9.

3. A. H. Al-Muslimawi and A. M. Shareef, *Numerical investigation of non-Newtonian inelastic flows through conical nozzles*, Journal of Education for Pure Science, vol. 13, no. 4, 2023. doi: 10.32792/utq.jceps.10.01.01.
4. J. R. Abdul-Jabbar, A. H. Al-Muslimawi, and I. A. Fadhel, *Computational Study of the Flow of Newtonian Fluid Through A Straight Channel and Lid-Driven Cavity*, Iraqi Journal of Science, vol. 64, no. 8, pp. 4043–4057, 2023. doi: 10.24996/ijs.2023.64.8.28.
5. K. Zheng, A. Raza, A. M. Abed, H. Khursheed, L. F. Seddek, A. H. Ali, and A. U. Haq, *New fractional approach for the simulation of (Ag) and (TiO2) mixed hybrid nanofluid flowing through a channel: Fractal fractional derivative*, Case Studies in Thermal Engineering, vol. 45, pp. 102948, 2023. doi: 10.1016/j.csite.2023.102948.
6. A. Raza, R. Ali, S. M. Eldin, S. H. Alfalqui, and A. H. Ali, *New fractional approach for CMC and water based hybrid nanofluid with slip boundary layer: Applications of fractal fractional derivative*, Case Studies in Thermal Engineering, vol. 49, pp. 103280, 2023. doi: 10.1016/j.csite.2023.103280.
7. S. Sivanandam and B. Marimuthu, *Numerical study on influence of inclination and sinusoidal heating on magneto-convection in an inclined lid-driven cavity*, Multidiscipline Modeling in Materials and Structures, vol. 19, no. 3, pp. 361–374, 2023. doi: 10.1108/MMMS-03-2022-0044.
8. F. Auteri, N. Parolini, and L. Quartapelle, *Numerical investigation on the stability of singular driven cavity flow*, Journal of Computational Physics, vol. 183, no. 1, pp. 1–25, 2002. doi: 10.1006/jcph.2002.7145.
9. A. F. Khalaf, F. L. Rashid, A. Rashid, A. Basem, and M. H. Abbas, *Numerical Analysis in a Lid-Driven Square Cavity with Hemispherical Obstacle in the Bottom*, Mathematical Modelling of Engineering Problems, vol. 9, no. 6, 2022. doi: 10.18280/mmep.090625.
10. M. R. Patel, J. U. Pandya, and V. K. Patel, *Numerical analysis of fluid flow behaviour in four-sided square lid-driven cavity using the finite volume technique*, International Journal of Applied and Computational Mathematics, vol. 8, no. 4, pp. 153, 2022. doi: 10.1007/s40819-022-01353-x.
11. M. H. Borbora, B. Vasu, and A. J. Chamkha, *A review study of numerical simulation of lid-driven cavity flow with nanofluids*, Journal of Nanofluids, vol. 12, no. 3, pp. 589–604, 2023. doi: 10.1166/jon.2023.1930.
12. M. Khalid, R. U. Haq, A. Alhushaybari, and E. A. Algehyne, *Lid driven flow and heat transfer due to various positions of slit in a square cavity: FEM approach*, International Communications in Heat and Mass Transfer, vol. 159, pp. 107951, 2024. doi: 10.1016/j.icheatmasstransfer.2024.107951.
13. H. R. Tamaddon–Jahromi, D. Ding, M. F. Webster, and P. Townsend, *A Taylor–Galerkin finite element method for non–Newtonian flows*, International Journal for Numerical Methods in Engineering, vol. 34, no. 3, pp. 741–757, 1992. doi: 10.1002/nme.1620340304.
14. A. J. Chorin, *Numerical solution of the Navier-Stokes equations*, Mathematics of Computation, vol. 22, no. 104, pp. 745–762, 1968. doi: 10.1090/S0025-5718-1968-0242392-2.
15. V. Ngamaramvaranggul and M. F. Webster, *Computation of free surface flows with a Taylor–Galerkin/pressure–correction algorithm*, International Journal for Numerical Methods in Fluids, vol. 33, no. 7, pp. 993–1026, 2000. doi: 10.1002/1097-0363(20000815)33:7¡993::AID-FLD40¿3.0.CO;2-A.
16. A. A. Al-Khashab, A. Al-Haboobi, and A. H. Al-Muslimawi, *Computational investigation of non-Newtonian inelastic flows in a 4:1 contraction based on artificial compressibility method*, Results in Control and Optimization, vol. 23, pp. 100730, 2026. doi: 10.1016/j.rico.2026.100730.
17. A. Al-Haboobi and A. H. Al-Muslimawi, *A New Algorithm For Solving Thermal Newtonian Flow In Axisymmetric Straight Channel*, Basrah Journal of Science, vol. 41, no. 3, pp. 399–418, 2023. doi: 10.29072/basjs.20230301.
18. A. Al-Haboobi, I. A. Fadhel, A. A. Sharhan, and A. H. Al-Muslimawi, *Computational simulation of compressible Newtonian flow past circular and square bluff bodies*, Ocean Systems Engineering, vol. 14, no. 4, pp. 315–330, 2024. doi: 10.12989/ose.2024.14.4.315.
19. A. Al-Haboobi and A. H. Al-Muslimawi, *Simulation of Newtonian Axisymmetric Thermal Channel Flow by Using a Developed Taylor–Galerkin/Pressure Correction Method*, International Journal of Applied and Computational Mathematics, vol. 11, no. 5, 2025. doi: 10.1007/s40819-025-02010-9.
20. J. H. Dymond and R. Malhotra, *The Tait equation: 100 years on*, International Journal of Thermophysics, vol. 9, no. 6, pp. 941–951, 1988. doi: 10.1007/BF01133262.
21. J. van Kan, *A Second-Order Accurate Pressure-Correction Scheme for Viscous Incompressible Flow*, SIAM Journal on Scientific and Statistical Computing, vol. 7, no. 3, pp. 870–891, 1986. doi: 10.1137/0907059.
22. F. A. Mohammed and A. H. Al-Muslimawi, *Numerical Study of Compressible and Weak Compressible Flows in Channel Based on Artificial Compressibility Method and Fully Artificial Compressibility Method*, Iraqi Journal of Science, vol. 64, no. 3, pp. 1331–1343, 2023. doi: 10.24996/ijs.2023.64.3.27.
23. F. M. White and J. Majdalani, *Viscous Fluid Flow*, vol. 3, McGraw-Hill, New York, 2006.
24. S. H. Al-Zaidi and A. Al-Haboobi, *Investigation of inelastic power-law model under thermal conditions by using a developed method*, Boletim da Sociedade Paranaense de Matematica, vol. 43, no. 1, pp. 1–11, 2025. doi: 10.5269/bspm.77563.